Asian Journal of Chemistry; Vol. 31, No. 1 (2019), 18-24

ASIAN JOURNAL OF CHEMISTRY

https://doi.org/10.14233/ajchem.2019.21647

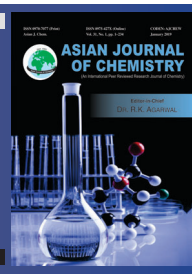

REVIEW

Metal Oxide based Chalcogenides Heterostructure Thin Film Photoanodes for Photoelectrochemical Solar Hydrogen Generation

S.M. HO[1,*], M.A. MAHADIK[2], J.S. JANG[2] and V.N. SINGH[3]

[1]Centre for Green Chemistry and Applied Chemistry, INTI International University, Putra Nilai 71800, Negeri Sembilan, Malaysia
[2]Division of Biotechnology, Advanced Institute of Environmental and Bioscience, College of Environmental and Bioresource Sciences, Chonbuk National University, Iksan 570-752, Republic of Korea
[3]Indian Certified Reference Materials Division, CSIR-National Physical Laboratory, Dr. K.S. Krishnan Road, New Delhi-110012, India

*Corresponding author: Tel: +606 7982000; E-mail: soonmin.ho@newinti.edu.my

Received: 13 August 2018; *Accepted*: 4 September 2018; *Published online*: 30 November 2018; AJC-19154

Thin films have been used for many applications. Hydrogen production from solar water splitting has been considered as a key solution to the energy and environmental issues. The tuned band gap alignments in metal chalcogenides/metal oxides heterostructure enable efficient separation of photogenerated electrons and holes, leading to the effective hydrogen production. We sensitize these structures by hydrothermal methods and evaluate the performance toward hydrogen generation. This work shows a brief overview of photoelectrochemical hydrogen production, progress and ongoing sprints. Here, different metal chalcogenides were deposited on metal oxides (TiO_2 and Fe_2O_3) in order to improve the photoelectrochemical performance by reducing recombination of photogenerated electron–hole pairs and facilitate hole transport at the metal chalcogenides/metal oxides/electrolyte interface. The study includes chalcogenides/metal oxides heterostructure designs and electrochemistry and solar hydrogen generation are brought together, illustrating the promise and challenge of photoelectrochemistry.

Keywords: Metal oxides, Photoelectrochemistry, Chalcogenides, Heterojunction, Hydrogen generation.

INTRODUCTION

Thin film technology plays a key role in almost all the areas includes electronics, optical coatings, superconducting films, magnetic films, environmental & energy, heat prevention & corrosion resistance, super hard coatings and solar cells [1-5]. For example, chalcogenide thin films used in photovoltaic cells (as absorbing material) because of appropriate band gap and high absorption coefficient value. Thin film coating can be classified according to coating thickness. The thin films can have different properties compared to bulk material. Common processes in recent thin-film technology include vacuum based [6-9] and non-vacuum based technology [10-14].

History of thin films in ancient times: Thin-film science and technology is all together one of the ancient art and the latest science. The element or gold is the first metal discovered more than 11,000 years ago [15]. It was used for decoration, making ornaments, religious artefacts because of its soft nature and prominently for business (symbol of wealth). The first inorganic thin films were made of gold having thickness less than 300 nm thick made by mechanical pressing on artifacts which found in Egypt [16,17], Bulgaria [18] and Europe [19] close to 5000 BC years approximately. Examples of which are found in early stone pyramids in Egypt. After the invention of battery by Alexandrai Volta in 18th century, deposition of thin films by electroplating was carried out.

Thin film preparation in the ancient era: Thin film deposition by gas phase reaction (chemical vapour deposition) started in 1649, solution–gel process (sol-gel) in 1885 and thin film deposition in atmosphere at the end of 19th century. However, the surface adhesion, roughness of the medium, the need of clean environment hindered processes to larger extent.

Evolution of vacuum technology: The vacuum (derived from Latin word *Vacuus*, means empty space) science started

in mid-1600 and most important achievement was by Italian mathematician and physicist Torricelli (1608-1647), who invented barometer for measuring atmospheric pressure and thus created vacuum [20]. In the year 1652, Otto von Guericke (1602-1686) of Germany invented a mechanical piston pump which could create a vacuum of 2 Torr [21,22]. Today with the scientific and manufacturing advances, vacuum pumps can achieve an ultrahigh vacuum with in a minimum interval of time, which is inevitable for the clean thin film depositions [23].

Modern thin film technology: The history in ancient times using gold beating and gilding for film preparation was not enough to complete because of the fact that surface preparation, cost and purity of gold, surface adhesion, reaction between metals used in the process (for example mercury as adhesion layers, copper *etc*.) should also be taken in to consideration. With the invention of vacuum pumps (mechanical pumps) in 17^{th} century, vapour phase deposition of thin films like sputtering in 1852, plasma enhanced chemical vapour deposition (CVD) in 1869 and evaporation in 1915 have started to dominate. The modern thin film technology addressed the generic issues using vacuum technology, crystallography, semi-conductor technology and surface science [23].

Properties: The size effects in thin film greatly influence the noted properties of thin films namely electrical properties, mechanical and optical properties, as reported by many researchers [24-33]. There are other important functional properties as well thin film can perform besides conventional properties.

The first and foremost experimental parameter to be measured for thin film materials is its thickness because thin-film properties usually are governed by on thickness. Microelectronic applications as well as optical coatings applications require more accurate measurement of thickness.

Light beam interferometry and ellipsometry are the two basic and important optical methods for measuring film thickness. The quantities which can be measured from the above measurements are index of refraction, thickness of few nanometer layer coatings, optical transmittance, reflectivity and absorbance and hence the energy band gap *etc*. Thickness can also be measured using mechanical methods namely stylus profilometer and quartz crystal micro balance.

Optical properties: Transmission and absorption spectra provide a clear idea of estimating the refractive index, thickness and also extinction coefficient values in thin films (semi conducting, metallic and insulating also). In particular, calculation of band gap of materials is very easy after analyzing the optical properties of thin films.

Optical behaviour of a thin metal film: Optical properties also influenced by the film structure, which in turn depends on deposition conditions. The substrate temperature, deposition rate and type of substrate also influence film properties. Films deposited at low rates will have more granular nature and sometimes epitaxial growth may also occur as reported [34].

Optical behaviour of a dielectric thin film: The optical behaviour of dielectric thin films is simpler than that of metal films. The dielectric thin films show lesser refractive index because of effects of granularity. After taking optical spectra of thin films, the refractive index, extinction coefficients and thickness can also be determined. If the bulk material is transparent at some wavelength, then its thin film counterpart will be much more transparent. Even a thin metal layer (Au) will become transparent to visible light. The optical constants that will be used as index of refraction, dielectric constant will be determined by Ellipsometry technique [35], interference methods [36] and other.

Conductivity properties: The electrical conductivity in general for all materials is given by relation:

$$\sigma = q.n.\mu \quad (1)$$

with q, n, μ are charge, carrier concentration and mobility respectively. If one of the dimensions of material is reduced, then the carrier concentration may change if the films are so thin that the system is identically equal to two-dimensional gas. When the thickness of film comes to the same order as mean free path of charge carriers, then mobility μ is going to reduces and hence the conductivity reduces. Bulk wire of good conductors like Al or Cu wire having a cross-sectional area of 1 mm^2, the maximum current density before it goes up in smoke is approximately a few 1.0 A/cm^2.

However, a thin layer having a cross-section of about 1 μm^2 can easily allow critical current density of greater than 10^5 A/cm^2, which is many orders of magnitude unexpectedly higher than the bulk value, making it possible for their use in integrated circuit. This is because volume to surface ratio of a thin film wire allows a much better transport of the heat produced in the wire to the large heat sink called as "substrate" and to the environment. Electrical conductivity and hence resistivity can be measured by four probe measurement set up and more accurate carrier concentration by Hall Effect measurement for thin film.

Mechanical properties: It is well known that stresses exist even though films (during growth) are not externally loaded, called as residual or internal stresses. These stresses effect adhesion, defects, perfection and formation of unique film surface growths such as hillocks.

The elastic moduli properties arise from atom to atom interaction between which often same in bulk as well as in thin film form. However, if the thin film is in the order of atomic level, thin in other words, the bonding situation is rigorously disturbed and leads to altering the elastic properties between bulk and thin films elastic moduli [37]. For example, the hardness (yield strength) of thin films could be larger than bulk values [38].

The reason will be as followed in taking in to consideration of many things. First one is dislocation density or the grain size. In case of thinner films, it is a bit of good news that they take lot of stress. It can also happen that film brittle in nature like Si can be deposited on silicon substrate in roll to roll deposition for many applications.

In case of nano structured thin films, mechanical properties namely elastic modulus and support very high residual stresses thin films. The same will be released through plastic deformation or thin film fracture. Both properties elastic and plastic deformation are important for thin film characterization.

Mechanical properties of thin film can be measured by tensile testing of free standing thin films and also by micro beam cantilever deflection technique. However, the easiest way is by means of nano indentation techniques, where no special sample preparation is required and tests can be executed speedily and economically favourable way [39].

Functional properties of thin films: Energy is the extraordinary source of technological, scientific and economic development of any country. Assuring energy sources for the societies need and further growing requirement is the foremost challenges for the next decades. In the present electronic world, power requirements for portable electronics can be taken care by thin film. Thermo electric generators and thin film all solid state batteries because thin film can be deposited on any substrate irrespective of it shape. Thin film thermoelectric generators and thin film batteries are portable devices, which can support power requirements of portable electronics.

Electrochemical properties of thin films: Lithium-ion battery materials can have deposited in thin film form in sequential deposition and can be possible to fabricate a thin film battery. Cyclic voltammetry (CV) and galvanostatic charge discharge cycling are major electrochemical properties to be measured for thin film electrodes using electrochemical methods. The schematic of thin film battery is shown below. The schematic of thin film battery [40] is shown in Fig. 1. The specific discharge capacity was calculated by using the following relation

$$\text{Specific capacity} = \frac{I \times t}{A \times f} \quad (2)$$

where I is charge-discharge current, t is the discharge time, A is area and f is the thickness of the film. The higher is the specific capacity, the best is the electrode which can be used for solid state battery application [41,42]. Cyclic voltammetry and galvanostatic charge discharge studies give evidence of electrochemical activity.

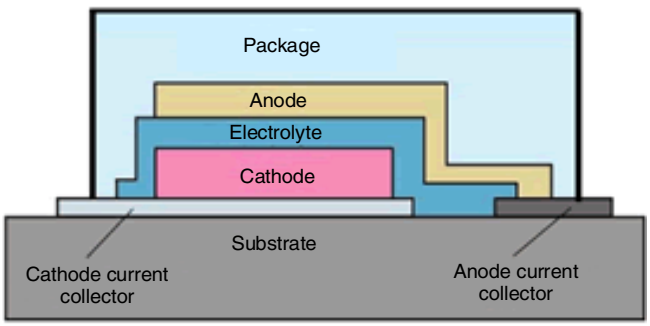

Fig. 1. Schematic of thin film battery

Thermo electric properties of thin films: Thermoelectric devices [43,44] contain many thermoelectric couples (Fig. 2) consisting of *n*-type thin films (containing free electrons as charge carriers) and *p*-type thin films (containing free holes as charge carriers) thermoelectric elements which are wired electrically in series and thermally in parallel.

Efficient utilization of solar energy could alleviate many energy and environmental issues in the coming years. Hydrogen, as a sustainable clean energy source, has attracted much attention over the past decade, because of high calorific potential, no waste production, recyclability and environmental-friendly property [45]. Since the discovery of the Honda-Fujishima effect, in a titanium dioxide (TiO_2) photoelectrochemical (PEC) cell, use of semiconductors for photocatalytic water splitting has become an important topic in many research fields where clean and renewable hydrogen (H_2) fuel can generated directly from solar irradiation [46]. Many effective photo catalysts have been developed; however, some of them only work in the ultraviolet (UV) region and few of them which having band gap around solar visible light but cannot have suitable band edge position for reducing water [47]. Fortunately, the semiconductor heterostructure provides a feasible method for integrating the merits of different materials into one single photoelectrode [48]. Due to their more suitable band edge positions than oxides and excellent performance for photocatalytic hydrogen production, some visible-light-responsive chalcogenides have been extensively studied [49,50]. However, the chalcogenide suffers from the photo corrosion issue and to overcome this drawback, it is highly desirable to fabricate hierarchical nanostructures with different band gaps and appropriate band positions materials. Even though, many methods have already been reported for synthesis of metal chalcogenites/metal oxides [51-54], they suffer from poor photoelectrochemical (PEC) stability owing to the hole-induced self-oxidative decomposition of the chalcogenides. For efficient photoelectrochemical H_2 evolution, efficient separation of the photogenerated electrons and holes is extremely important. This work reports to design, synthesize and evaluate a new metal oxide nanorod based chalcogenides photoanode material, which will have a superior combination of materials properties that will permit high efficiency tandem photoelectrochemical and improved stability of devices. Also we understand the phenomena and the charge transport mechanism happening in the surface modified heterostructure photoanodes used for solar water splitting.

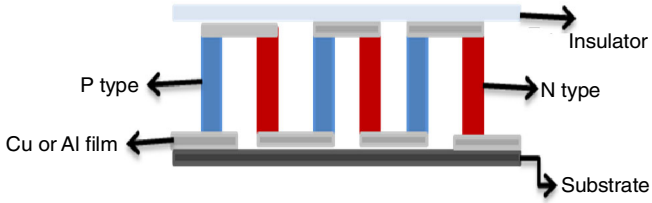

Fig. 2. Schematic of thin film thermos electric generator

EXPERIMENTAL

All photoelectrochemical experiments were conducted in a three-electrode system with the metal oxide coated ZT as the working electrode, platinum (Pt) wire as the counter electrode and silver/silver chloride (Ag/AgCl) as the reference electrode, using an approach as in an earlier work [55]. The photocurrent–voltage (J–V) curves were performed using a portable potentiostat (COMPACTSTAT.e, Ivium, Netherland) equipped with an electrochemical interface and impedance analyzer facility. A simulated one sun illumination (100 mW cm^{-2}) using a solar simulator (Abet Technologies). The electrolyte consisted of 0.1 M Na_2S and 0.02 M Na_2SO_3 in deionized water. An air-tight three-electrode photoelectrochemical cell with an aqueous solution electrolyte, Ag/AgCl reference electrode and a Pt wire counter electrodes were used for gas

chromatography. The optimized metal chalcogenides/metal oxide photoelectrode was used as working electrode and biased at 1.23V *versus* reversible hydrogen electrode (RHE). Before the light irradiation, N_2 gas was purged through the photoelectrochemical cell for 1 h to complete the removal of the dissolved oxygen in the electrolyte. The amount of oxygen and hydrogen evolved from the photoelectrode and the Pt counter electrode were measured using gas chromatograph equipped with a thermal conductivity detector (TCD) and a molecular sieve 5 Å packed column.

RESULTS AND DISCUSSION

Fabrication of metal oxide nanorod (TiO_2 and Fe_2O_3) thin film photoanodes: Titanium dioxide (TiO_2) nanorods and hematite (Fe_2O_3) nanorods were synthesized on fluorine doped tin oxide (FTO) by a facile hydrothermal process according to the literature [56,57]. However, metal oxide loaded $ZnIn_2S_4$/TiO_2/FTO glass was prepared by a simple method as reported by Mahadik and co-workers [58]. Fig. 3(a,b) shows the field emission scanning electron microscopy (FESEM) image of the hydrothermally-prepared TiO_2 nanorod arrays and $ZnIn_2S_4$/TiO_2 (ZT). The top view shows that uniformly and densely packed, vertically-aligned TiO_2 nanorods which were further covered by continuous metal oxide loaded $ZnIn_2S_4$ layer nanosheet. Fig. 3c indicates in the voids among the TiO_2 nanorods. This change in the surface morphology of ZT after the metal oxide coatings (TiO_2, SiO_2 and Al_2O_3, further reported as TZT, SZT and AZT) may be responsible for the providing more surface area of electrode coming in contact with electrolyte, more scattering of light and hence, the enhanced absorption of the film. To study the effect of the type of metal oxides on the structure of ZT electrodes the photoelectrochemical performance was studied using a three-electrode system. Fig. 3d shows the photocurrent density-potential curves of pristine ZT, TZT, AZT and SZT. The photocurrent density of the SZT film was approximately 0.786 mA cm^{-2}, which is two times greater than that of pristine ZT (0.370 mA cm^{-2}) and more than 1.5 times greater than that of TZT and AZT. The hydrogen evolution (Fig. 3e) linearly increased with the solar light irradiation time and the total amount of H_2 produced by SZT was 96 µmol after 3 h (32 µmol h^{-1}). The photostability of the photoanode was also investigated during the hydrogen production. Fig. 3f is schematic of charge transfer mechanism in metal oxide coated ZT photoanode. The potential difference of the conduction band edge of $ZnIn_2S_4$ and TiO_2 transfers the photogenerated electrons from the conduction band (CB) of $ZnIn_2S_4$ to that of TiO_2; then, the electrons migrate to the surface of the counter electrode where they can reduce H^+ to hydrogen. Alternatively, because of more positive valance band (VB) edge of TiO_2 than that of $ZnIn_2S_4$, the holes in the valance band of the TiO_2 transfer to $ZnIn_2S_4$ and react with the SO_3^{2-}, S^{2-} ions in the electrolyte and produces the S_2^{2-} and $S_2O_3^{2-}$ ions [59]. Thus, in order to reduce the recombination losses in the ZT photoanodes, a metal oxide was coated onto the ZT. The main function of the metal oxide layer is to retard interfacial charge recombination [60]. Therefore, the deposited metal oxide acts as a barrier for the interfacial electron transfer, suppressing recombination and to increase the photocurrent [61].

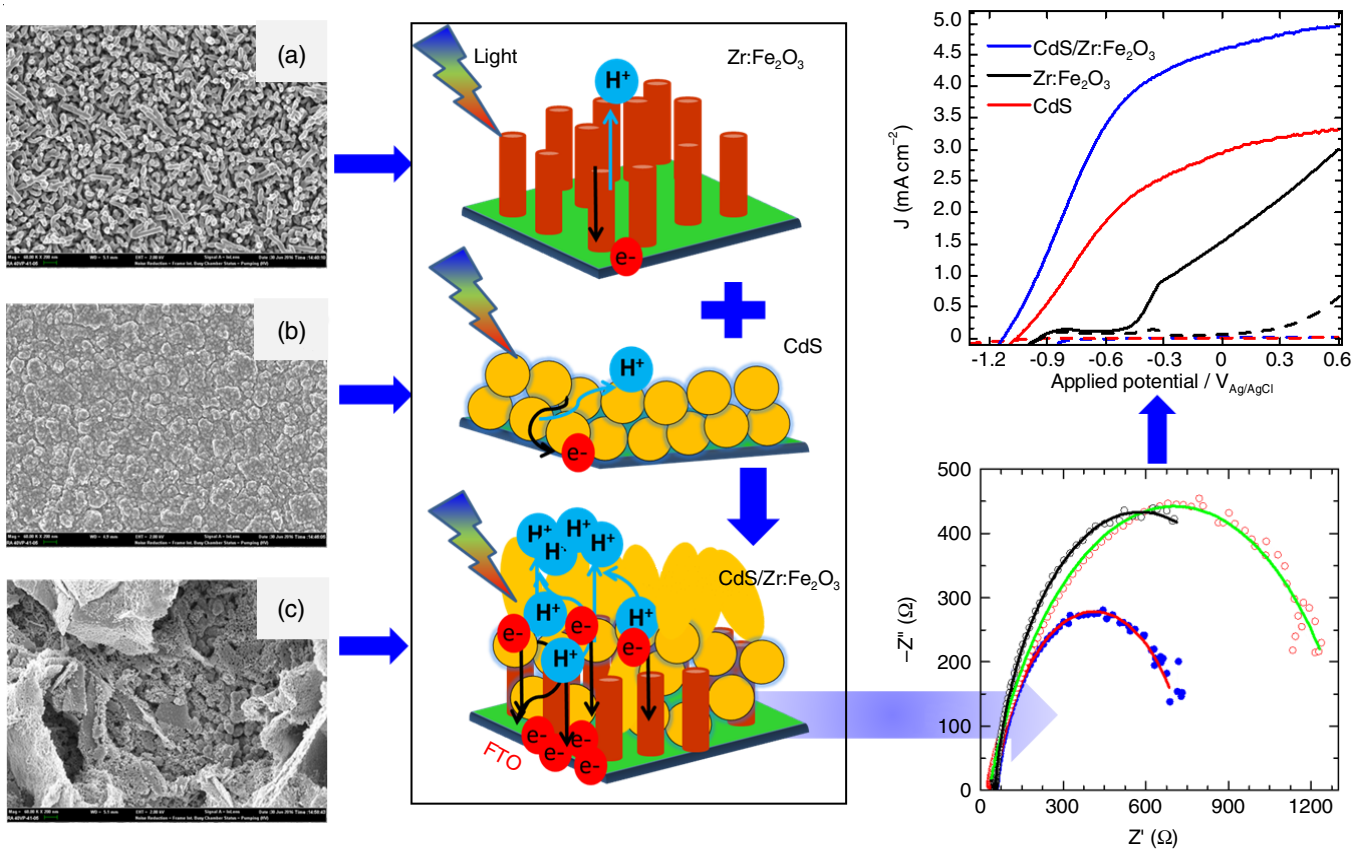

Fig. 3. FESEM top view images of the $Zr:Fe_2O_3$, CdS and $CdS/Zr:Fe_2O_3$ nanorod array heterojunction, corresponding schematic illustration of the synergistically improved PEC performance of $CdS/Zr:Fe_2O_3$ heterojunction

Fabrication of CdS/Fe_2O_3 heterojunction thin film photoanodes: Mahadik and co-workers [62] have described the synthesis of CdS layer on one dimensional (1D) Zr:Fe_2O_3/FTO by using hydrothermal method. The heterojunction between CdS and Fe_2O_3 nanorods is another promising strategy for the purpose to improve photoelectrochemical performance, which might be useful for effective way to harvest visible light and promote charge separation, leading to a high photocatalytic efficiency for hydrogen (H_2) generation [63,64]. However, despite the efficiency of the nanocomposite powder catalysts are still far from reaching industrial viability hence fabrication thin films of CdS/1D Zr doped Fe_2O_3 nanorod array (CdS/Zr:Fe_2O_3) on fluorine doped tin oxide (FTO) *via* facile hydrothermal route for synergistic study on photoelectrochemical performance is of great importance. To improve the stability and photoelectrochemical performance of CdS/Zr:Fe_2O_3 nanorod arrays heterojunction, a layer of Al_2O_3 was also deposited on the surface of a photoanode. The mechanism of photogenerated charge transport in CdS/1D Zr:Fe_2O_3 heterojunction and role of Al_2O_3 on CdS surface is also proposed. As shown in Fig. 4a, Zr:Fe_2O_3 nanorods (NR) are well aligned and vertically oriented to the surface of the FTO, whereas, CdS grains are decorated on a FTO shows smooth surface (Fig. 4b). However, in CdS/Zr:Fe_2O_3 heterojunction, CdS flakes like structure forms on Zr:Fe_2O_3 nanorods (Fig. 4c). This helps to efficient light absorption and transport of photogenerated charges by reducing the resistances occurred in CdS nanograins. Thus, CdS flake enlarges the surface area of flakes and leads to an improved charge transfer and thereby, the photoelectrochemical performance.

To study the origin of improved photoelectrochemical performance of heterojunction, the UV-visible absorption spectra were measured and as shown in Fig. 5a. It clearly, shows irregularly shaped fused CdS nanoparticles on FTO show a weak absorption intensity compared with Zr:Fe_2O_3. However, for the wavelength shorter than 500 nm, the absorption intensity of CdS/Zr:Fe_2O_3 heterojunction is more enhanced than the absorption edge of pristine Zr:Fe_2O_3. Thus, the absorption spectra of CdS/Zr:Fe_2O_3 heterojunction show the combined effect of both CdS and Zr:Fe_2O_3, which is helpful for the enhancement of photoelectrochemical performance. To confirm the effect of the Al_2O_3 concentration on the photoelectrocatalytic stability of CdS/Zr:Fe_2O_3 heterojunction, various concentrations of Al_2O_3 such as 5, 10 and 15 mM coated CdS/Zr:Fe_2O_3 heterojunctions.

Fig. 5(b) shows the linear sweep voltammetric (LSV) scans of different concentrations of Al_2O_3 coated CdS/Zr:Fe_2O_3 heterojunctions. It is observed that the highest photocurrent density of 5.0 mA cm^{-2} for 10 mM Al_2O_3 loading. This increased photocurrent density for the coated Al_2O_3 surface over the uncoated Al_2O_3 surface is due to the decrease in the recombination of electron-holes and increased interfacial charge transfer at the photoelectrode/electrolyte interface [65]. Fig. 5(c) shows a comparison of the photocatalytic H_2 production activities of the uncoated and Al_2O_3 coated CdS/Zr:Fe_2O_3 heterojunction photoanods. Al_2O_3 coated films exhibit an improved photoelectrochemical stability than uncoated CdS/Zr:Fe_2O_3. This is due to the co-catalyst (Al_2O_3) treatment plays a dual role: the passivation of surface states and the reduced charge recombination at CdS surface by effectively tunneling them in to electrolyte. When the photoanode is illuminated [Fig. 5(d)], the photoexcited electrons generated at Al_2O_3 and CdS were collected at the FTO substrate along the Zr:Fe_2O_3 nanorod arrays and then moved to the Pt electrode *via* the external circuit. At

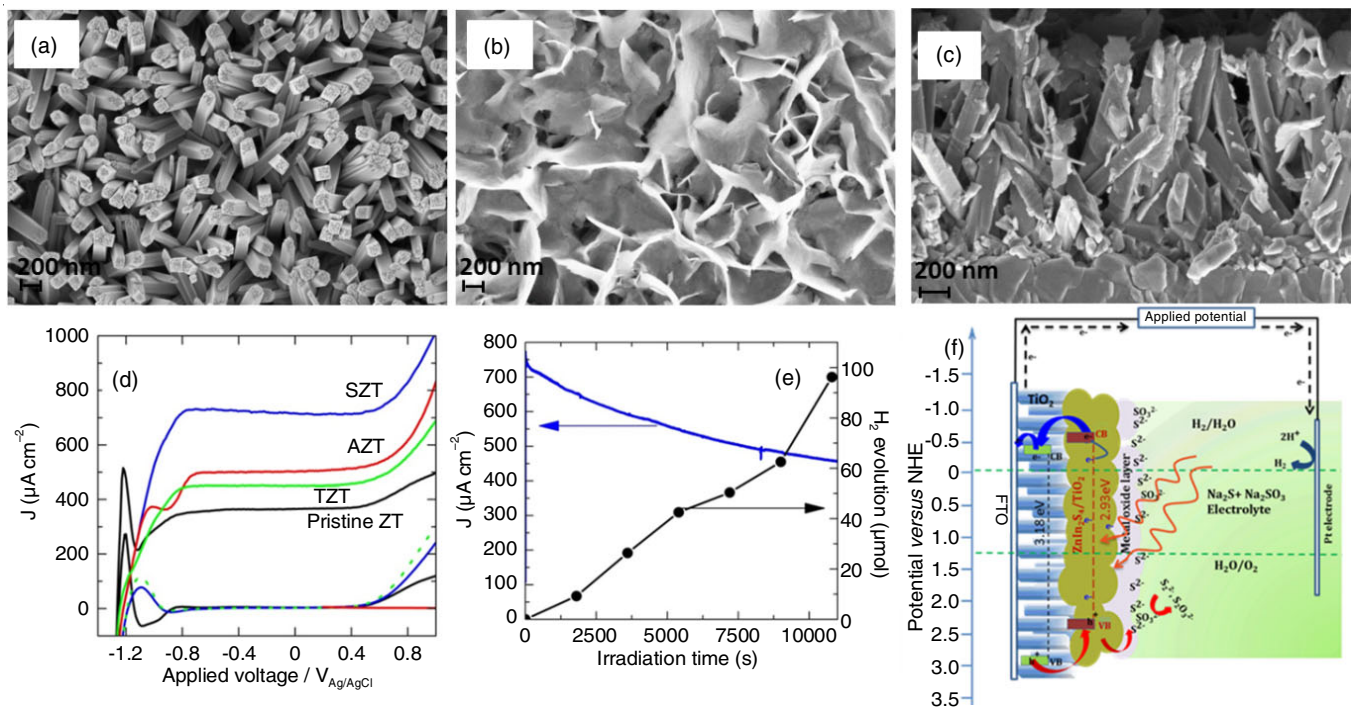

Fig. 4. SEM images of the surface view (a, b) of TiO_2, SZT and cross-section (c) of SZT thin films, respectively, (d) Photocurrent potential characteristics of ZT, TZT, AZT and SZT photoelectrodes, (e) Evolution of H_2 and photocurrent density as a function of time measured at 0.1 V *versus* Ag/AgCl using SZT as a photoelectrode under 100 mW cm^{-2} light illumination and (f) Schematic of charge transfer mechanism in metal oxide coated ZT photoanode

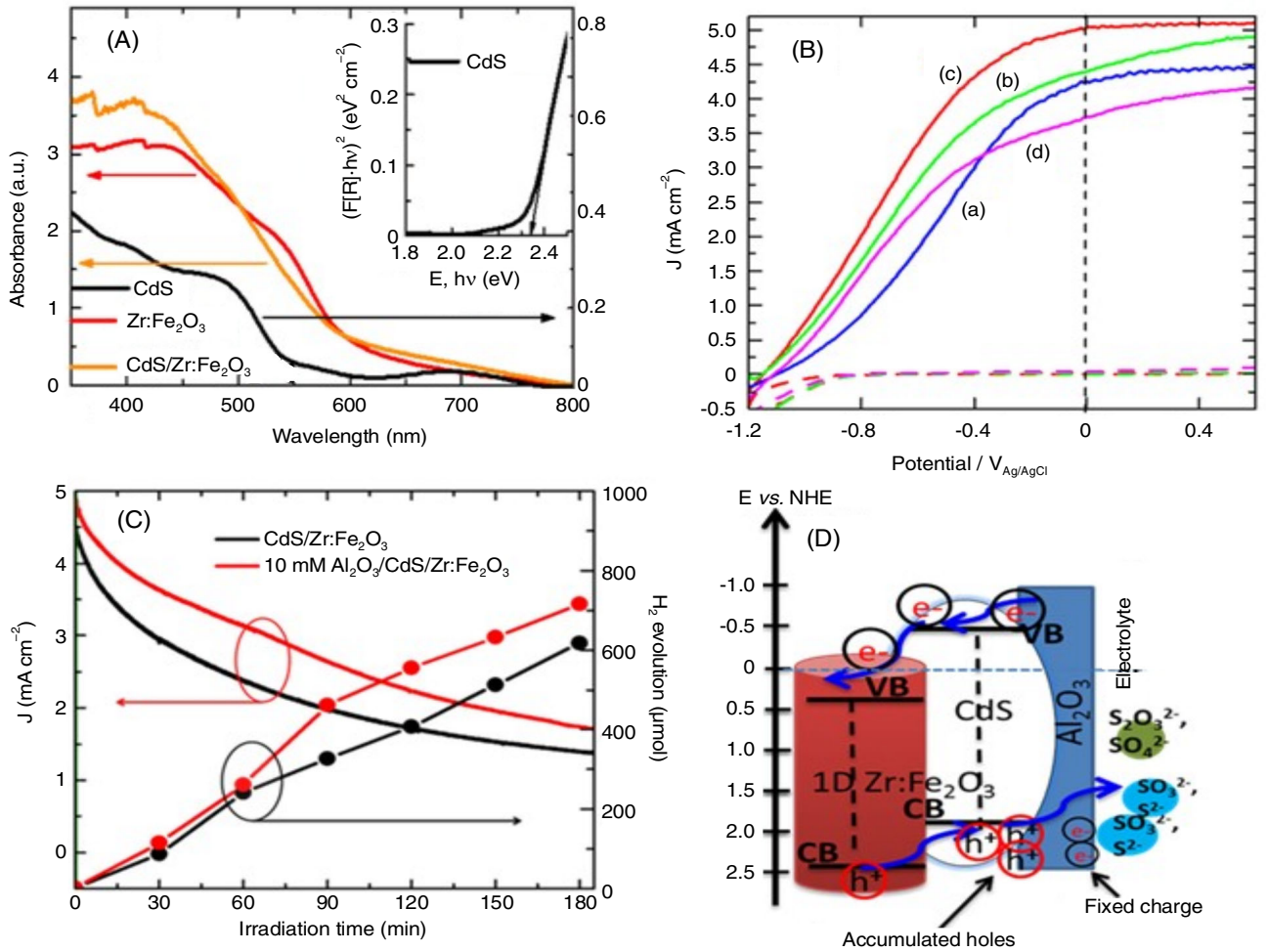

Fig. 5. (A) Tauc plots of CdS nanograin thin film on the FTO substrates, (B) Linear sweep voltammetric scans (a) 0 mM, (b) 5 mM, (c) 10 mM and (d) 15 mM Al_2O_3 coated CdS/Zr:Fe_2O_3 heterojunctions, (C) Hydrogen generation *vs.* irradiation time plots of uncoated CdS/Zr:Fe_2O_3 and 10 mM Al_2O_3 coated CdS/Zr:Fe_2O_3 heterojunction photoanodes recorded in an aqueous solution containing 0.1 M Na_2S and 0.02 M Na_2SO_3 (pH ≈ 11.5) at 0 V *vs.* Ag/AgCl, (D) possible mechanism of photogenerated charge separation at Al_2O_3 coated CdS/Zr:Fe_2O_3 heterojunction

the same time, the photogenerated holes due to the presence of the Al_2O_3 layer on CdS surface interact with the SO_3^{2-} and S^{2-} radicals in the Na_2S/Na_2SO_3 sacrificial reagent and produce $S_2O_3^{2-}$ and SO_4^{2-} ions [66,67]. Thus, the remarkable improvement in the photocurrent of heterojunction thin films due to co-catalysts, however, further improvement of photostability is needed which will help to use these thin film for future solar energy conversion.

Conclusion

In summary, hydrogen generation *via* water splitting is a promising field, which has made great progress the last decades. The noble metal chalcogenides/metal oxides hybrid nanostructures were successfully synthesized *via* hydrothermal approach and the various deposition parameters (concentration, hydrothermal temperature and deposition times) were optimized as well. The hybrid nanostructures were immersed in solution containing different chemicals in order to stabilize the samples. One of the advantages with TiO_2 and Fe_2O_3 nanorods in general is its photoelectrochemical stability.

ACKNOWLEDGEMENTS

One of the authors (Ho SM) is thankful to the INTI International University for supporting this work. This research grant for (MA Mahadik & JS Jang) was supported by Korean National Research Foundation (Nano-Material Fundamental Technology Development, 2016M3A7B4909370) and the Korea Research Fellowship Program through the National Research Foundation of Korea (NRF), funded by the Ministry of Science and ICT (2017H1D3A1A02014020). Also, this work was supported by the Korea Ministry of the Environment as Eco-Innovation project (2016000140001).

CONFLICT OF INTEREST

The authors declare that there is no conflict of interests regarding the publication of this article.

REFERENCES

1. S.M. Ho, *Asian J. Chem.*, **27**, 3851 (2015); https://doi.org/10.14233/ajchem.2015.19013.
2. K. Anuar, S.M. Ho and W.T. Tan, *Eur. J. Appl. Sci.*, **3**, 75 (2011).
3. H. Chen, S. Fu, S. Wu, H. Wu and C. Shih, *Mater. Lett.*, **169**, 126 (2016); https://doi.org/10.1016/j.matlet.2016.01.030.
4. T. Daniel, J. Henry, K. Mohanraj and G. Sivakumar, *Mater. Res. Express*, **3**, 116401 (2016); https://doi.org/10.1088/2053-1591/3/11/116401.
5. K. Noraini, K. Anuar, S.M. Ho and H.A. Abdul, *Dig. J. Nanomater. Biostruct.*, **5**, 975 (2010).
6. K. Benyahia, A. Benhaya and M.S. Aida, *J. Semicond.*, **36**, 103001 (2015); https://doi.org/10.1088/1674-4926/36/10/103001.

7. N. Memarian, S.M. Rozati, I. Concina and A. Vomiero, *Materials*, **10**, 773 (2017); https://doi.org/10.3390/ma10070773.
8. B.M.S. Sahuban, R. Chandramohan, T.A. Vijayan, K.S. Saravana, K.S.R. Sri, M. Jayachandran and A. Ayeshamariam, *J. Mater. Sci. Eng.*, **5**, 297 (2016); https://doi.org/10.4172/2169-0022.1000297.
9. J.M. Kephart, R.M. Geisthardt and W.S. Sampath, *Prog. Photovoltaic*, 23, 1484 (2015); https://doi.org/10.1002/pip.2578.
10. T. Dhandayuthapani, M. Girish, R. Sivakumar, C. Sanjeeviraja and R. Gopalakrishnan, *Appl. Surf. Sci.*, **353**, 449 (2015); https://doi.org/10.1016/j.apsusc.2015.06.154.
11. E. Yücel and S. Kahraman, *Ceram. Int.*, **41**, 4726 (2015); https://doi.org/10.1016/j.ceramint.2014.12.021.
12. M.V. Morales-Gallardo, A.M. Ayala, M. Pal, M.A. Cortes Jacome, J.A. Toledo Antonio and N.R. Mathews, *Chem. Phys. Lett.*, **660**, 93 (2016); https://doi.org/10.1016/j.cplett.2016.07.046.
13. A. Kassim, S.M. Ho, W.T. Tan, S. Atan, K. Zulkefly and N. Saravanan, *Chiang Mai Univ. J. Nat. Sci.*, **7**, 318 (2008).
14. S. Monohorn, S.M. Ho, K. Anuar, S. Nagalingam and W.T. Tan, *J. Sci. Eng. Technol.*, **6**, 126 (2010).
15. M. Stanczak, A Brief History of Copper, Cambridge Scientific Abstracts: Bethesda, MD (2005).
16. D. Klemm, R. Klemm and A. Murr, *J. Afr. Earth Sci.*, **33**, 643 (2001); https://doi.org/10.1016/S0899-5362(01)00094-X.
17. T. James, *Gold Bull.*, **5**, 38 (1972); https://doi.org/10.1007/BF03215160.
18. C. Renfrew, *Antiquity*, **52**, 199 (1978); https://doi.org/10.1017/S0003598X00072197.
19. C. Renfrew, *Antiquity*, **45**, 275 (1971); https://doi.org/10.1017/S0003598X00069799.
20. M.J. Sparnay, Adventures in Vacuum, North Holland Publishing: Eindhoven, The Netherlands (1992).
21. T.S. Baynes, The Encyclopaedia Britannica: A Dictionary of Arts, Sciences, Literature and General Information, Encyclopaedia Britannica: New York, vol. 19, p. 246 (1888).
22. T.E. Conlon, Thinking about Nothing: Otto von Guericke and the Magdeburg Experiments on the Vacuum, The Saint Austin Press: London (2011).
23. M. Ohring, Material Science of Thin films, Academic Press, edn 2 (2002).
24. S.S. Tulenin, A.V. Pozdin, K.A. Karpov, D.A. Novotorkina and M.S. Rogovoy, *Asian J. Chem.*, **30**, 1655 (2018); https://doi.org/10.14233/ajchem.2018.21307.
25. J. Zhu, X. Zhang, Y. Zhu and S.B. Desu, *J. Appl. Phys.*, **83**, 1610 (1998); https://doi.org/10.1063/1.366872.
26. Y. Choi and S. Suresh, *Acta Mater.*, **50**, 1881 (2002); https://doi.org/10.1016/S1359-6454(02)00046-0.
27. H.D. Espinosa and B.C. Prorok, *J. Mater. Chem.*, **38**, 4125 (2003); https://doi.org/10.1023/A:1026321404286.
28. E.I. Rogacheva, O.N. Nashchekina and S.I. Menshikova, *J. Electr. Mater.*, **46**, 3842 (2017); https://doi.org/10.1007/s11664-017-5481-1.
29. M. Tallarida, C. Das and D. Schmeisser, *Beilstein J. Nanotechnol.*, **5**, 77 (2014); https://doi.org/10.3762/bjnano.5.7.
30. J.H. Park, J. Ahn, K.J. Yoon, H. Kim, H.-I. Ji, J.-H. Lee, S.M. Han and J.-W. Son, *J. Electrochem. Soc.*, **165**, F671 (2018); https://doi.org/10.1149/2.0961809jes.
31. A.Z. Simoes, C.S. Riccardi, L.S. Cavalcante, A.H.M. Gonzalez, E. Longo and J.A. Varela, *Mater. Res. Bull.*, **43**, 158 (2008); https://doi.org/10.1016/j.materresbull.2007.02.011.
32. J. Kim, S. Qin, W. Yao, Q. Niu, M.Y. Chou and C.-K. Shih, *PNAS*, **107**, 12761 (2010); https://doi.org/10.1073/pnas.0915171107.
33. J.H. Mohd, K. Anuar, S.M. Ho, W.T. Tan, Y.R. Mohd, H.A. Abdul and N. Saravanan, *Kuwait J. Sci. Eng.*, **37**, 63 (2010).
34. R. Sennett and G.D. Scott, *J. Opt. Soc. Am.*, **40**, 203 (1950); https://doi.org/10.1364/JOSA.40.000203.
35. W.E.J. Neal and R.W. Fane, *J. Phys. E Sci. Instrum.*, **6**, 409 (1973); https://doi.org/10.1088/0022-3735/6/5/001.
36. O.S. Heavens, *Rep. Prog. Phys.*, **23**, 301 (1960); https://doi.org/10.1088/0034-4885/23/1/301.
37. D.A. Hardwick, *Thin Solid Films*, **154**, 109 (1987); https://doi.org/10.1016/0040-6090(87)90357-9.
38. T.P. Weihs, S. Hong, J.C. Bravman and W.D. Nix, *J. Mater. Res.*, **3**, 931 (1988); https://doi.org/10.1557/JMR.1988.0931.
39. S.P. Baker and W.D. Nix, *J. Mater. Res.*, **9**, 3131 (1994); https://doi.org/10.1557/JMR.1994.3131.
40. www.ornl.gov.
41. J.B. Bates, N.J. Dudney, B. Neudecker, A. Ueda and C.D. Evans, *Solid State Ion.*, **135**, 33 (2000); https://doi.org/10.1016/S0167-2738(00)00327-1.
42. N.J. Dudney, *Mater. Sci. Eng. B*, **116**, 245 (2005); https://doi.org/10.1016/j.mseb.2004.05.045.
43. G.J. Snyder and E.S. Toberer, *Nat. Mater.*, **7**, 105 (2008); https://doi.org/10.1038/nmat2090.
44. P. Gokhale, B. Loganathan, J. Crowe, A. Date and A. Date, *Energy Procedia*, **110**, 281 (2017); https://doi.org/10.1016/j.egypro.2017.03.140.
45. J.A. Turner, *Science*, **285**, 687 (1999); https://doi.org/10.1126/science.285.5428.687.
46. H. Kato, K. Asakura and A. Kudo, *J. Am. Chem. Soc.*, **125**, 3082 (2003); https://doi.org/10.1021/ja027751g.
47. X. Chen, S. Shen, L. Guo and S.S. Mao, *Chem. Rev.*, **110**, 6503 (2010); https://doi.org/10.1021/cr1001645.
48. G. Ai, H. Li, S. Liu, R. Mo and J. Zhong, *Adv. Funct. Mater.*, **25**, 5706 (2015); https://doi.org/10.1002/adfm.201502461.
49. H. Yan, J. Yang, G. Ma, G. Wu, X. Zong, Z. Lei, J. Shi and C. Li, *J. Catal.*, **266**, 165 (2009); https://doi.org/10.1016/j.jcat.2009.06.024.
50. F. Cao, W. Shi, L. Zhao, S. Song, J. Yang, Y. Lei and H. Zhang, *J. Phys. Chem. C*, **112**, 17095 (2008); https://doi.org/10.1021/jp8047345.
51. X. Wang, G. Liu, L. Wang, Z.G. Chen, Q. Lu and H.M. Cheng, *Adv. Energy Mater.*, **2**, 42 (2012); https://doi.org/10.1002/aenm.201100528.
52. J. Lee, T.G. Kim, H. Choi and Y. Sung, *Cryst. Growth Des.*, **7**, 2588 (2007); https://doi.org/10.1021/cg070588m.
53. G. Ai, R. Mo, H. Xu, Q. Chen, S. Yang, H. Li and J. Zhong, *J. Power Sources*, **280**, 5 (2015); https://doi.org/10.1016/j.jpowsour.2015.01.071.
54. K. Cheng, X. Han, J. Meng, S. Wang and Z. Du, *RSC Adv.*, **5**, 11084 (2015); https://doi.org/10.1039/C4RA15204B.
55. M.A. Mahadik, P.S. Shinde, M. Cho and J.S. Jang, *J. Mater. Chem. A Mater. Energy Sustain.*, **3**, 23597 (2015); https://doi.org/10.1039/C5TA07454A.
56. B. Liu and E.S. Aydil, *J. Am. Chem. Soc.*, **131**, 3985 (2009); https://doi.org/10.1021/ja8078972.
57. A. Annamalai, A. Subramanian, U. Kang, H. Park, S.H. Choi and J.S. Jang, *J. Phys. Chem. C*, **119**, 3810 (2015); https://doi.org/10.1021/jp512189c.
58. M.A. Mahadik, P.S. Shinde, M. Cho and J.S. Jang, *Appl. Catal. B*, **184**, 337 (2016); https://doi.org/10.1016/j.apcatb.2015.12.001.
59. W. Kim, T. Tachikawa, D. Monllor-Satoca, H. Kim, T. Majima and W. Choi, *Energy Environ. Sci.*, **6**, 3732 (2013); https://doi.org/10.1039/c3ee42151a.
60. E. Palomares, J.N. Clifford, S.A. Haque, T. Lutz and J.R. Durrant, *J. Am. Chem. Soc.*, **125**, 475 (2003); https://doi.org/10.1021/ja027945w.
61. X. Gao, D. Guan, J. Huo, J. Chen and C. Yuan, *Nanoscale*, **5**, 10438 (2013); https://doi.org/10.1039/c3nr03198e.
62. M.A. Mahadik, A. Subramanian, J. Ryu, M. Cho and J.S. Jang, *Dalton Trans.*, **46**, 2377 (2017); https://doi.org/10.1039/C6DT04472G.
63. M. Yin, C.-K. Wu, Y. Lou, C. Burda, J.T. Koberstein, Y. Zhu and S. O'Brien, *J. Am. Chem. Soc.*, **127**, 9506 (2005); https://doi.org/10.1021/ja050006u.
64. A. Hameed, T. Montini, V. Gombac and P. Fornasiero, *J. Am. Chem. Soc.*, **130**, 9658 (2008); https://doi.org/10.1021/ja803603y.
65. M.A. Mahadik, A. Subramanian, H.S. Chung, M. Cho and J.S. Jang, *ChemSusChem*, **10**, 2030 (2017); https://doi.org/10.1002/cssc.201700140.
66. P. Lv, W. Fu, H. Yang, H. Sun, Y. Chen, J. Ma, X. Zhou, L. Tian, W. Zhang, M. Li, H. Yao and D. Wu, *CrystEngComm*, **15**, 7548 (2013); https://doi.org/10.1039/c3ce40863a.
67. H. Park, W. Choi and M.R. Hoffmann, *J. Mater. Chem.*, **18**, 2379 (2008); https://doi.org/10.1039/b718759a.